Maximum lift predictions of a realistic commercial aircraft in landing configuration

Bier, N.* and Rohlmann, D.,†
German Aerospace Center (DLR), D-38108 Braunschweig, Germany

Abstract

Within task three "Numerical Simulations" in the project "HINVA - High Lift INflight Validation" extensive numerical verification studies based on a CAD model of DLR's A320-232 "Advanced Technology Research Aircraft" in landing configuration are carried out. Therein special attention is paid to the effect of certain geometric features of the high-lift system, such as slat tracks, de-icing pipe etc. Also the empennage and a model of both the operational engine and a through flow nacelle are included in the geometry. The numerical simulations are carried out using the Spallart-Allmaras turbulence model which represents DLR's current best-practice for such applications. In this paper the structure of the task is presented along with results of initial numerical simulations assessing the influence of the slat tracks, the de-icing pipe and the TFN in comparison to the operational engine.

Nomenclature

α	angle of attack
ATRA	Advanced Technology Research Aircraft
C_L	lift coefficient
deg	degree
lcts	lift counts (1 lct = 0.01)
Ma	Mach number
Re	Reynolds number
TC	test case
TFN	through-flow nacelle

1 Introduction

Three-element high-lift systems consisting of slats, main wing and Fowler-type of flaps are well-established as an efficient compromise between a desired gain in lift and complexity of the mechanical system[1]. In principle the aerodynamic interactions between the three elements are

*Research Scientist, Institute of Aerodynamics and Flow Technology, niko.bier@dlr.de.
†Research Scientist, Institute of Aerodynamics and Flow Technology, david.rohlmann@dlr.de.

understood[2]. However, because of the highly complex geometry of realistic high-lift systems and the disturbance of the principal mechanisms by vortex-dominated and detached flows at high angles of attack the CFD-based prediction of high-lift performance remains a challenging task. During the last years these capabilities have improved continuously[3]. And although a good agreement between CFD-predictions and wind tunnel measurements has been achieved in general, the prediction of stall mechanisms, increments in lift due to changes in geometry and flight conditions and the prediction of absolute values of maximum lift and the associated angle of attack still remains a challenging task. This is especially the case for realistic flight Reynolds numbers. Following experiences shared by the industry, the offset between high lift performance measured in real flight compared to predictions based on wind tunnel measurements or CFD simulations is still not as precise as it should be.
Against this background, the project "HINVA - High Lift INflight Validation"[4] aims at narrowing the gap between predictions and measured high-lift performance of future civil transport aircrafts to the accuracy which is desired from the aerodynamics design point of view. This does not only apply to the maximum lift itself but also to the corresponding angle of attack. In its four work packages WP 1 "ATRA Flight Tests", WP 2 "ETW Windtunnel Experiments", WP 3 "Numerical Simulations" and WP 4 "Simulation Strategy", HINVA aims not only at identifying the key drivers responsible for deviations in maximum lift predictions, but especially at quantifying their impact on maximum lift and its associated angle of attack. The results will be evaluated in WP 4 with the main emphasize on defining a future simulation-strategy suitable to precisely predict high-lift performance in an efficient, robust and industrial relevant way.

Figure 1: DLR's A320-232 Advanced Technology Research Aircraft 'ATRA'.

DLR's "Advanced Technology Research Aircraft" (ATRA), an Airbus A320-232 equipped with two International Aero Engines IAE V2527-A5 engines, is used in HINVA for stall flight tests (Figure 1). In addition a halfmodel for cryogenic wind tunnel tests in the European Transsonic Windtunnel (ETW) will be build based on the measured flight shape at $C_{L,max}$-conditions[4]. A detailed CAD geometry of the ATRA is also available for CFD simulations. This offers the unique possibility to directly compare the results of all three methods for $C_{L,max}$-determination both in terms of maximum lift itself and the associated angle of attack α_{max}, respectively. Furthermore the flow topology and the pressure distributions can be compared at the exactly the same positions on all elements of the high-lift wing.

2 Geometric Representation

The CAD geometry used is a precise representation of the ATRA in landing configuration[4] with fully deployed slats and flaps, the deployed aileron, the horizontal and vertical stabilizers and the operational IAE V2500 engine with nacelle strake. The model is further equipped with flap track fairings and pylon end fairings, slat tracks, the slat horn and the de-icing pipe. The designed twist distribution for the flight case is already taken into account in the geometry representation of all three elements of the high lift wing ("Flight twist"), whereas no additional bending is modeled ("Jig Bending"). For CAD preparation the commercial software packages CATIA V5, Release 18[5], and CADfix[6] were used.

2.1 Slat Cove Elements

Since it is known from other investigations[8] that a significant influence of the slat tracks on the pressure distribution on the suction side of the main wing may exist, only simplifications inevitable in order to generate a mesh were applied to the representation of the slat tracks in the CAD model. Mostly this applies to the intersections of the tracks with the main wing and the slat itself. In 2 one can see that in reality the cavities in the wing D-nose are slightly larger in size than the tracks and although the effect of those cavities on maximum lift might not be disregarded in all cases, especially when they are not properly sealed towards the wing suction side, they were not included in the main CAD geometry. However, it is considered to assess their influence on maximum lift for some selected cases in a later part of the project. The same considerations apply to the de-icing pipe which is also represented without the cavities in the slat cove and the wing's D-nose. Another minor simplification is applied by not explicitly modeling the slat tracks' sealing plates close to the cove. Since these plates are in close vicinity of the slat cove in an area of supposedly detached flow, this simplification seems acceptable.

Figure 2: Real and discretized geometry of the slat tracks and the de-icing pipe.

2.2 Flap related modifications

Further simplifications in the geometric representation of the ATRA were made at the flap track fairings (FTF) where the details of the kinematic itself have not been modeled and the flap is kind of free-flying since the shape of the fairing is assumed to have a significantly larger impact as the additional disturbance of the kinematic elements themselves.
At the flap-fuselage intersection the CAD geometry differs slightly from the real geometry: at the real aircraft the gap between flap and fuselage grows constantly in chordwise direction and is closed by a rubber sealing at the inboard side of the inboard flap. Since meshing of such small gaps is difficult applying hybrid meshes with prismatic elements to resolve boundary

layers, the gap was slightly increased to allow prismatic layers to grow on both sides. Following the investigations of Keller[9] this simplification is not expected to have any notable impact on the overall solution but leads in this case to an important increase of grid quality.

2.3 Engine

An important driver of maximum lift and a possible cause for deviations in maximum lift predictions by flight tests, wind tunnel tests or CFD simulations might be the engine thrust which not only contributes partly to the lift but also can interact with the complex aerodynamics of the high-lift system, especially the fully deployed flaps. The wind tunnel model however is equipped with a through-flow nacelle (TFN) which not only lacks thrust but also shows a differing geometry because of an intake modification and an increased nozzle area usually applied to TFN wind tunnel models. In order to assess the influence of the engine thrust the baseline CAD model is equipped with the operational IAE V2500 engine, whereas a modified CAD model is equipped with the wind tunnel model's TFN with increased exhaust area and intake modification. A numerical simulation then offers the possibility to directly compare the results and quantify the impacts of thrust and geometry on $C_{L,max}$ and α_{max}.

3 Grid generation

The baseline grid for the configuration with maximum geometrical detail was created using the commercial grid generator CENTAUR[7]. By the placement of different sources and the use of anisotropic stretching the grid resolution of the surface as well as in the grid domain has been adjusted aiming to achieve a high spatial resolution with as few grid nodes as possible. Since a complete modular approach as suggested in [10] for all geometric details to be investigated seems desirable but nonetheless unfeasible, for the placement of the volume sources the same strategy as in former investigations[3] was applied: Starting from the setup with the most complex geometry, all test cases with less geometric details were meshed using the same sources. This approach supposedly leads to comparable grids for all configurations and assumable minimizes grid influences in the simulations. For the surface resolution an anisotropic stretching in spanwise direction of two was applied for the wing parts outboard of the engine to reduce the overall number of points. In the inboard wing section the anisotropic stretching was reduced to unity since the complex flow physics and possible interactions between various vertical flow systems with the boundary layers may well show significant changes in spanwise direction. All trailing edges were modeled as blunt trailing edges and resolved with at least two cells to decouple the pressure and the suction side in the dual grid metric of the TAU Code[11, 12]. In most cases the trailing edges could be meshed with structured hexahedrons, again in order to reduce the overall number of points. In order to resolve the vortices arising from e.g. the slat horn or the nacelle strake, the initial source placement was adapted based on preliminary simulations for different angles of attack between 7 deg and α_{max}. Figure 3 shows the final surface grid of the baseline configuration (top left) along with a view on the inboard wing section (top right), the inboard flap-fuselage junction (bottom left) and the V2500 nacelle with strake (bottom right).

In order to be able to use one single grid of a specific configuration throughout the whole range of the flight test campaigns' Mach and Reynolds number variations, 40 layers of prismatic elements were used, having a first spacing that ensures values of $y^+ < 1$ for all cases, except for the suction peaks on the slat at high angles of attack where values of $y^+ < 3$ can be reached. To avoid chopping of the prismatic layers the surface resolution in areas with high curvature

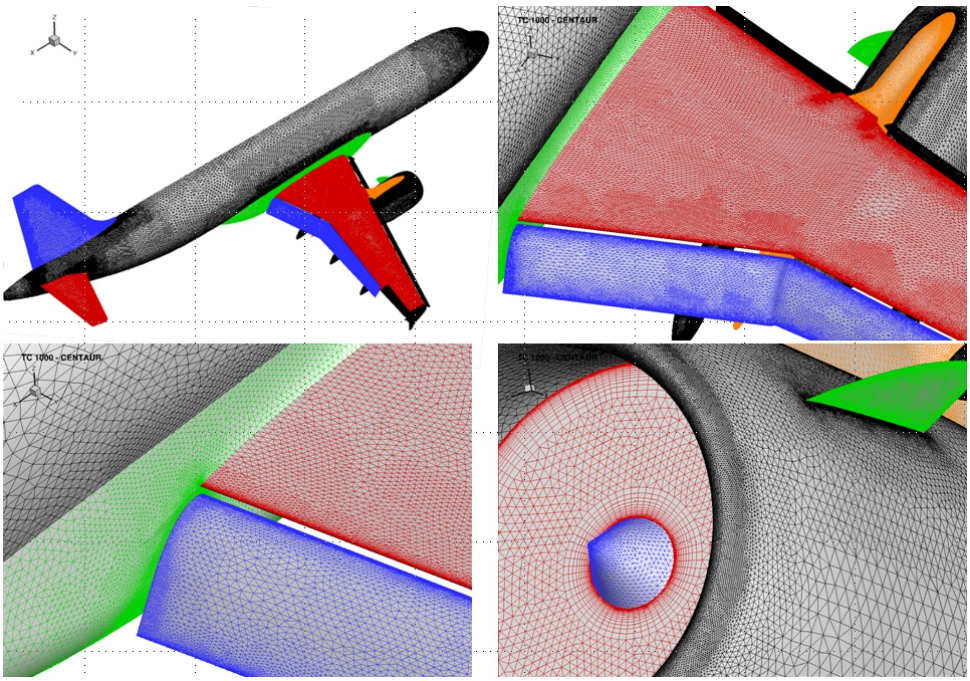

Figure 3: Final surface grid of the ATRA in landing configuration.

was increased. A stretching ratio for the prismatic elements was chosen in such a way that the final height is approximately twice as high as the final boundary layer on the main wing trailing edge for the lowest Reynolds number. With this approach grids of the ATRA in landing configuration a minimum of not less than 30 prismatic layers was achieved in all cases. The outer block's farfield boundary-condition is located at a distance of 100 half spans from the aircraft. Depending on the actual geometric complexity, the final grids consist of 68 to 81 million grid points in total.

4 Numerical Approach

The DLR TAU Code[11, 12] is a Navier-Stokes solver for the simulation of viscous and inviscid flows around general complex geometries. The solver is based on the finite volume method and uses a dual-grid approach, where the flowvariables are associated with the vertices of the original grid. The solver can handle different cell types and can be used on structured and unstructured (hybrid) grids. Generally, a semi-structured grid layer above surfaces is used to resolve boundary layers, whereas the rest of the computational domain is filled with an unstructured grid. The solver computes the fluxes with a second-order central scheme or one of various upwind schemes with linear reconstruction for second-order accuracy. Time integration is performed by either applying an explicit, multistage Runge-Kutta scheme or an implicit, lower-upper symmetric Gauss-Seidel (LU-SGS) scheme. Turbulent flows are modeled using different Spalart-Allmaras, $k-\omega$ or Reynolds stress turbulence models (RSM). For transitional flows, laminar regions can be designated by the definition of polygon lines on the surface of the geometry and prescribing the maximum height of the laminar region over the surface. For these computations, the turbulent production terms are suppressed in the laminar flow area. For convergence acceleration multiple techniques like e.g. residual smoothing, local time stepping and different multigrid approaches can be applied.
Based on experience at DLR as well as on results from the first AIAA Highlift prediction workshop[13, 14] for the baseline simulations the Spallart Allmaras turbulence model[15] with

robust numerical settings accordingly to current DLR best practice along with the second-order central scheme with matrix dissipation was used. For time integration the implicit backward Euler LUSGS scheme was applied. With respect to convergence behavior a three level multigrid acceleration was used when possible. In a later phase of the project the influence of both more sophisticated settings and the highest-fidelity physical model available in the TAU Code, a differential RSM (SSG/LLR-) turbulence model[16] will be assessed, the latter in particular because of its potential rather to resolve than to model the vortical flow systems which dominate both maximum lift and the stall behavior of the ATRA.
All polar computations were started from scratch at a moderate angle of attack of $\alpha = 7.0$ deg within the linear part of the lift curve. Based on a converged solution at each angle of attack the subsequent one was simulated. The angle of attack was increased by $\Delta\alpha = 1.0$ deg in the linear part and by $\Delta\alpha = 0.5$ deg in the non-linear part. For each angle of attack between 20.000 and 40.000 cycles were simulated before a converged solution was obtained. Figure 4 shows exemplarily the convergence history for Testcase (TC) 1000 without slat cove elements for a medium-high angle of attack in the linear part of the lift curve (left) and one near maximum lift (right). It is important to notice that especially for the medium-high angle of attack not only before 7.500 cycles the beginning of a separation at the wing tip can be noticed in the force coefficients as well as in density and turbulence residuals. A converged solution is obtained after 25.000 cycles. However, for the high angle of attack already after 7.500 cycles the solution is converged with fluctuations in lift within $\Delta C_L = 0.03$ from the steady mean value. For even higher angles of attack the magnitude of the oscillations increases some but for pre-stall conditions a steady mean value was always obtained.

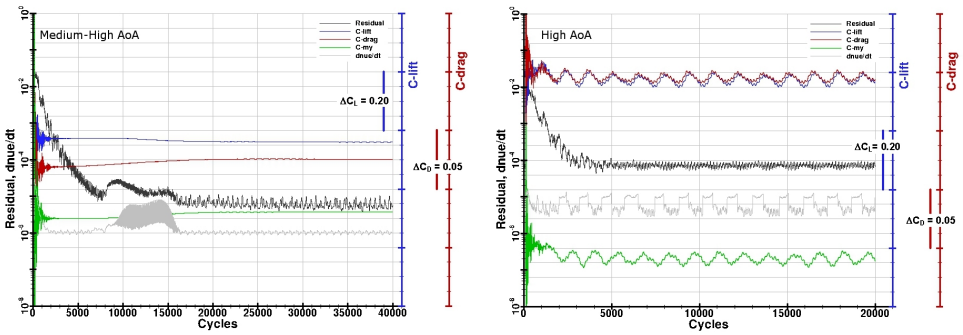

Figure 4: Examples of convergence history for TC 1000.

5 Results

For validation purposes a comprehensive matrix of more than 100 test cases (TC) were defined for flight and wind tunnel tests as well as for numerical simulations, including variations in configuration, geometric details, Mach and Reynolds numbers, etc. Not included in the matrix are additional numerical cases due to variations of numerical settings like e.g. the turbulence model. It is obvious that it is for practical reasons impossible to investigate the whole matrix in full amount. Therefore, based on initial CFD simulations and results from the first flight test, only the assumable most relevant test cases will be chosen for comparison and validation. Against this background initial polar computations with the SA turbulence model have been carried out in the first phase of HINVA prior to the flight tests in order to investigate the influence of the slat tracks and the de-icing pipe and the effect of the operational engine on $C_{L,max}$ compared to the TFN.

5.1 Global Results

The results of the initial polar computations are shown in Figure 5. All configurations show very similar lift predictions in the linear part of the lift curve, each without variations in lift over the last cycles per angle of attack. In the non-linear part and near maximum lift however, the predictions differ in terms of maximum lift itself as well as in the associated angle of attack. The deviations from a mean value still lie within the desired prediction accuracy and don't exceed values of $\Delta C_{L,max} < 0.07$ for maximum lift and $\Delta\alpha_{max} < 0.5$ deg for the associated angles of attack.

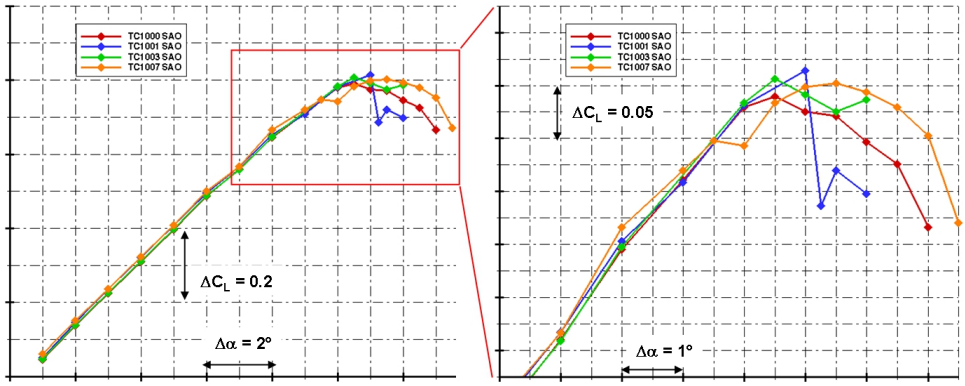

Figure 5: Initial polar computations for TCs 1000, 1001, 1003 and 1007.

A comparison between TC 1001 without any slat cove elements (blue), TC 1000 with slat tracks (red) and TC 1003 with slat tracks and de-icing pipe (green) shows - as expected - an earlier and less abrupt stall for the configurations with elements. In addition to these findings TC 1003 (green) exceeds TC 1000 (red) in maximum lift by 1.6 lift counts (lcts) against the expected trend while the lift oscillations over the last two periods in convergence history add up to 4.3 lcts. Since the lift predictions are quite similar for the linear part, a major grid dependency seems unlikely but is nonetheless possible. It is also possible that the global flow-history over all angles of attack plays a role in determining the actual lift coefficient for a specific angle of attack. So far for this case analysis is still ongoing and no final assessment is possible. For higher angles of attack at the end of the linear part of the lift curve TC 1007 with TFN (orange) shows an somewhat unexpected 'dip' which results in an approx. 1 deg delayed stall. The main reason for this dip is a loss of circulation on the flap in the wake of the TFN compared to the cases with operational engine. As a consequence in the case with TFN the pressure rise on the main wing has to be higher than with operational engine, which leads to additional loss of overall lift for these angles of attack. The absolute $C_{L,max}$ however remains nearly unaffected, as the stall pattern itself remains nearly unaffected (see section 5.2).

5.2 Stall Patterns and Vortical Flow Systems

Although $C_{L,max}$ and α_{max} differ for the investigated configurations, the stall patterns are very similar. Figure 6 shows them exemplarily based on the pressure distributions and skin frictions lines for TC 1001 without slat cove elements for three different points on the lift curve.

At low angles of attack and within the linear part of the lift curve (top right) the flow on the flap is separated over a wide spanwise extension while the flow on the main wing is mostly attached. Near the wingtip however, comparatively small areas of detached flow can be

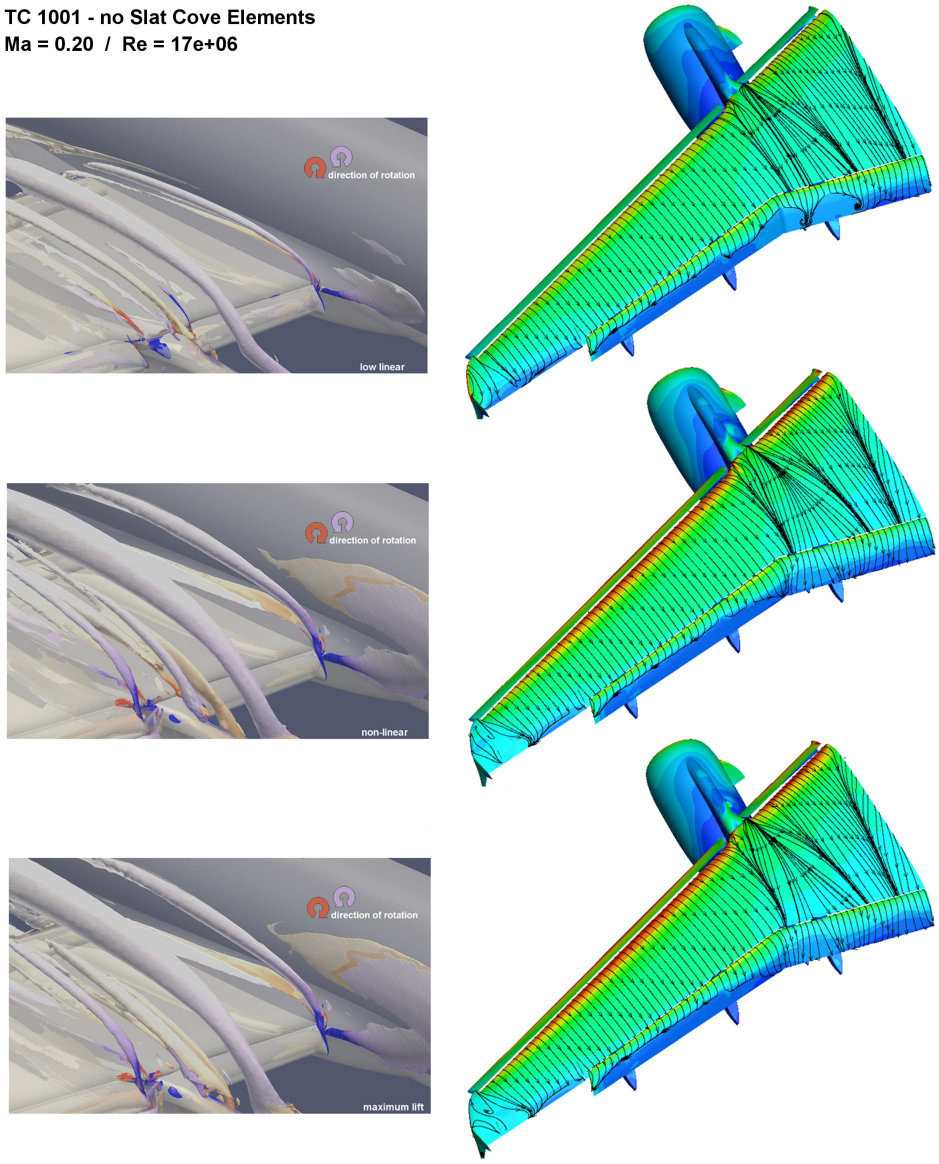

Figure 6: Initial polar computations for TCs 1000, 1001, 1003 and 1007.

observed. The vortical flow systems which will supposedly govern stall later on, e.g. nacelle and strake vortex, slathorn vortex, etc., are well resolved (top left). With increasing angle of attack in the non-linear part of the lift curve (middle) the flow on the inboard flap is more and more attached which leads to an overall increase in lift, even if the flow on the outer parts of the wing is detached. Also an increased loading and possible separations on the inboard part of the inboard flap at the root junction can be assumed. Again the vortical flow systems are well resolved and because of the increased loading also two vortices emerging from both edges of the slat in the cut-out region of the pylon become visible. The lower pictures in Figure 6 show maximum-lift-conditions. One can see that breakdown in lift starts gradually in the wake of the nacelle due to separations at the wing trailing edge, even though the flow at the inboard wing trailing edge is weakened as well. This stall pattern is also observed for TC 1007.
However, since an inboard nacelle strake is mounted on the engine, experience from other investigations[3] and literature[20] would suggest a breakdown in lift possibly starting at the inboard wing trailing edge near the fuselage. This corroborates the assumption that probably some flow features are resolved inadequately, e.g. the nacelle strake might not be fully oper-

ational in the CAD representation. Then again, at least many of the important vortical flow systems are well resolved over a wide range of angles of attack - and even at post-stall conditions - which does not favor the assumption of an insufficient grid resolution, inadequate physical or numerical modeling, etc. Since for this special aircraft with the IAE V2500 engine and a 40 deg flap deflection in landing configuration no detailed information about the stall pattern is available at DLR so far, the question remains to which degree the numerical predictions resemble the real aircraft's maximum-lift behavior.
By now this question impressively corroborates the HINVA-approach: A significant enhancement of $C_{L,max}$-prediction capabilities can only be achieved if all three pillars 'Flight Test', 'Wind Tunnel Test' and 'Numerical Simulation' work together in a joint effort on the same configurational basis.

6 Conclusion

In this paper we presented the results of preliminary numerical predictions of the maximum lift and the stall behavior of DLR's A320-232 "ATRA" in landing configuration. The simulations were carried out within the task "Numerical Simulations" of the project "HINVA - High Lift INflight Validation". The CAD model for the numerical simulations is very precise and the numerical grids that were generated resolve very well the assumable important flow phenomena dominating maximum lift. First results show well resolved vortex systems and predict stall onset due to flow separations emerging from the main wing trailing edge in the wake of the nacelle. The variations in predicted maximum lift and the associated angle of attack lie within the desired prediction accuracy.

Acknowledgments

The research work discussed in the paper is funded as part of the German Aeronautical Research Program LuFo IV. The authors are grateful to be selected to receive the funding for the present research project. Special thanks to all involved HINVA partners for their engagement and the technical contributions.

References

[1] Rudolph, P.K.C.: "High-Lift Systems on Commercial Subsonic Airliners". NASA CR 4746, 1996.

[2] Smith, A.M.O.: "High-Lift Aerodynamics". AIAA 6th Aircraft Design, Flight Test and Operations Meeting, Paper 74-939, 1974.

[3] v.Geyr, H. and Schade, N.: "CFD Prediction of Maximum Lift Effects on Realistic High-Lift-Commercial-Aircraft-Configurations within the European project EUROLIFT II". 25th AIAA Applied Aerodynamics Conference, Paper 2007-4299, 2007.

[4] Rudnik, R. and Reckzeh, D. and Quest, J.: "HINVA - High lift INflight VAlidation - Project Overview and Status". 50th AIAA ASM, Paper 2012-0106, 2012.

[5] Dassault Systemes: "CATIA V5 R18". www.3ds.com/products/catia.

[6] Intl. TechneGroup Inc.: "CADFix". www.transcendata.com/products/cadfix.

[7] CentaurSoft: "CENTAUR Software". http://www.centaursoft.com.

[8] Rudnik, R. and Ronzheimer, A.: "Numerical Investigation of the Flow around different Slat Tracks of a Swept HighLift Wing Segment". Notes on Numerical Fluid Mechanics and Multidisciplinary Design, Vol. 87, 2002, pp. 58-65.

[9] Keller, D.: "Numerical Investigation of Vortex and Separation Behavior on a Future Civil Transport Aircraft in High-Lift Configuration". Diploma Thesis, RWTH Aachen, 2010.

[10] Acheson, K. and Kornegay, B. and Lau, H.-F.: "Influence and Control of Unstructured Volume Meshes for Enhanced Fidelity Performance Predictions". AIAA paper 2011-3984, 2011.

[11] Schwamborn, D. and Gerhold, T. and Heinrich, R.: "The DLR TAU-Code: Recent Applications in Research and Industry". In Wesseling et al. (Eds.): "Proceedings of the European Conference on Computational Fluid Dynamics". ECCOMAS, 2006.

[12] Gerhold, T.: "Overview of the Hybrid RANS Code TAU". In "MEGAFLOW - Numerical Flow Simulation for Aircraft Design", Heidelberg, 2005, pp. 81-92.

[13] Crippa, S. and Melber-Wilkending, S. and Rudnik, R.: "DLR Contribution to the First High Lift Prediction Workshop". AIAA paper 2011-938, 2011.

[14] Rumsey, C. et al.: "Summary of the First AIAA CFD High-Lift Prediction Workshop". Journal of Aircraft, Vol. 48, No. 6, 2011, pp. 2068-2079.

[15] Spalart, P. and Allmaras, S.: "A One-Equation Turbulence Model for Aerodynamic Flows". AIAA paper 1992-439, 1992.

[16] Eisfeld, B.: "Numerical Simulation of Aerodynamic Problems with the SSG/LRR-Reynolds Stress Turbulence Model Using the Unstructured TAU Code". In: "Notes on Numerical Fluid Mechanics and Multidisciplinary Design". Vol. 96, 2007, pp. 356-363.

[17] Krumbein, A. and Krimmelbein, N. and Schrauf, G.: "Automatic Transition Prediction in a Hybrid Flow Solver-Part 1: Methodology and Sensitivities". Journal of Aircraft, Vol. 46, No. 4, 2009, pp. 1176-1190.

[18] Schrauf, G.: "COCO: A Program to Compute Velocity and Temperature Profiles for Local and Nonlocal Stability Analysis of Compressible, Conical Boundary Layers with Suction". ZARM, Center of Applied Space Technology and Microgravity, 1998.

[19] Schrauf, G.: "LILO 2.1. User's Guide and Tutorial". Tech. report, GSSC Technical Report 6, originally issued Sep. 2004, modified for Version 2.1., 2006.

[20] Haines, A.: "Scale Effects at High Lift and Low Speeds". In Young, A. (Edt.): "Scale Effects on Aircraft and Weapon Aerodynamics". AGARD-AG 323, 1999, pp. 27-65.